AIAA JOURNAL
Vol. 47, No. 4, April 2009

Hilbert Transform and Its Engineering Applications

Huageng Luo,* Xingjie Fang,† and Bugra Ertas‡
GE Global Research Center, Niskayuna, New York 12309

DOI: 10.2514/1.37649

The Hilbert transform is useful in calculating instantaneous attributes of a time series, especially the envelope amplitude and instantaneous frequency. The instantaneous envelope is the amplitude of the complex Hilbert transform; the instantaneous frequency is the time rate of change of the instantaneous phase angle. These properties can be applied to identify dynamic characteristics of a linear as well as a nonlinear system. However, the conventional discrete Hilbert transform, which is based on fast Fourier transform and inverse Fourier transform, has shown the lack of accuracy for time-derivative calculations. In this paper, we first introduce the Hilbert transform and its applications to the nonlinear system parameter identification. Then we address the practical issues in applying the Hilbert transform to engineering applications. To increase the accuracy of the envelope detection, we propose a Hilbert transform technique based on local-maxima interpolation. Analyses and simulations are carried out to demonstrate the advantages of the proposed technique. Finally, we employ the proposed local-maxima-interpolation technique in identifying the nonlinear dynamic characteristics of industrial examples.

Nomenclature

A	=	amplitude of the analytic function X
$H[\cdot]$	=	Hilbert transform
$H^{-1}[\cdot]$	=	inverse Hilbert transform
h_0	=	viscous damping coefficient
m, c, k	=	mass, damping, and stiffness of a dynamic system
P	=	Cauchy principal value
t	=	time
t_n	=	exact time when envelope and signal intersect
t_{na}	=	approximation of t_n
X	=	analytic function of x
x	=	displacement response
$\bar{x}$	=	Hilbert transform of x
$\dot{x}$	=	velocity response
$\ddot{x}$	=	acceleration response
θ	=	phase of the analytic function X
δ	=	logarithmic decrement
ω	=	instantaneous frequency
ω_0	=	undamped natural frequency

I. Introduction

THE Hilbert transform is widely used in radio communication engineering for amplitude modulation and demodulation. In mechanical dynamics, the Hilbert transform has been found to be applicable to vibration signals as well. One of the early applications was investigated by Simon and Tomlinson [1]. They provided a tool for a nonlinear detection method from the measured frequency-response function based on the fact that the frequency-response function of a linear system is invariant under a Hilbert transform.

Another application of the Hilbert-transform-based approach is manifested in the time domain. For a signal with a single tone, its Hilbert transform result is a signal that is 90 deg out of phase with the input. The original signal and the Hilbert transform formulate a complex analytic signal. The phase and the magnitude of the analytic signal are defined as the instantaneous phase and envelope, respectively, in which both are functions of time. The time derivative of the phase results in the instantaneous frequency. For a response signal that comes from a linear mass–damper–spring system impulse response, the frequency and damping ratio can be easily identified from this Hilbert transform approach. It has been demonstrated that this technique possesses some advantages, especially when the frequency-domain resolution is limited [2].

The monocomponent frequency requirement in the time-domain Hilbert transform is a limitation in its wide application to complicated engineering problems. However, the empirical mode decomposition (EMD) method proposed by Huang et al. [3] expanded the usage of the Hilbert-transform-based approach to many practical applications. This method analyzes a signal by decomposing it into so-called intrinsic mode functions. In conjunction with the Hilbert transform, this can be used for analyzing linear as well as nonlinear and nonstationary signals [4]. Later, Feldman [5] proposed a Hilbert vibration decomposition method (HVD) under the following assumptions:

1) The underlying vibration is formed by the superposition of quasi-harmonics functions.

2) The envelopes of each vibration component differ.

3) The total length of the vibration data includes several longest periods of the corresponding slowest component.

More recently, a detailed comparison between the EMD and the HVD was presented by Feldman [6].

Once the monocomponent signal is obtained, within certain restrictions, the time-domain Hilbert transform can be extended to identify modal parameters, such as frequency and damping, of nonlinear systems. Feldman [7,8] proposed the FREEVIB and the FORCEVIB methods to study instantaneous modal parameters (natural frequency, damping ratio, and their dependencies on vibration amplitude) from free- and forced-vibration responses, respectively. Allara et al. [9] used a similar approach to investigate the blade root damping, which is inherently nonlinear. More recently, Luo et al. [10] and Fang et al. [11] used the Hilbert transform to identify the nonlinear dynamic characteristics of granular dampers.

Both methods proposed by Feldman [7,8] require the use of the first and second derivatives of the fundamental variables (i.e., the derivatives of the instantaneous phase and the envelope). Although it is possible to do such numerical derivations for analytical or numerical simulation data, it may suffer from severe distortion/error when dealing with experimentally obtained data in practical

Presented as Paper 2196 at the 49th AIAA/ASME/ASCE/AHS/ASC Structures, Structural Dynamics, and Materials Conference, Schaumburg, IL, 7–10 April 2008; received 20 March 2008; revision received 4 December 2008; accepted for publication 23 December 2008.

*Mechanical Engineer, Structural Mechanics and Dynamics Laboratory, Building KW, Room D212A. Member AIAA.

†Mechanical Engineer, Structural Mechanics and Dynamics Laboratory, Building KW, Room D212B. Member AIAA.

‡Mechanical Engineer, Structural Mechanics and Dynamics Laboratory, Building KW, Room D150U. Member AIAA.

engineering problems. The experimentally obtained data inevitably contain noise and the noise can be easily amplified through numerical derivations. In many engineering cases, the noise can be the dominant signal component after the second derivative. Although, in theory, the time derivatives can be replaced by using the fast Fourier transform (FFT), multiplication in the frequency domain, and inverse FFT [12], the errors due to the end effect in the data cannot be eliminated. This end effect will affect the accuracy of the identification results, especially in highly damped cases. Furthermore, because the widely used discrete Hilbert transform (DHT) algorithm is based on the FFT and the inverse FFT approach as well [13], the assumptions used in the discrete-time Fourier transform (DTFT) can also introduce errors in the envelope detection.

In this paper, we introduce an alternative approach to the DHT. Rather than using the FFT and inverse-FFT-based Hilbert transform to get the signal envelope, we use a local maxima interpolation (LMI)-based approach to calculate the signal envelope.

The paper is organized as follows: In Sec. II, the fundamentals of Hilbert transform and its application in parameter identification are discussed. In Sec. III, practical issues and solutions of the discrete Hilbert transform in engineering applications are outlined. The LMI-based enveloping-detection technique is described in this section as well. Analyses and simulations are carried out in this section to demonstrate the improvement of the LMI method over the conventional method. In Sec. IV, the developed (LMI) process is applied to real engineering problems, the identification of the dynamic characteristics of a cantilevered blade, and a nonlinear wire-mesh damper. Finally, conclusions are drawn from the present study in Sec. V.

II. Hilbert-Transform-Based Parameter Identification

A. Hilbert Transform and Instantaneous Frequency Identification

Let $x(t)$ be a real-valued signal. The Hilbert transform $\bar{x}(t)$ is given as [14]

$$\bar{x}(t) = H[x(t)] = \frac{-1}{\pi} P \int_{-\infty}^{\infty} \frac{x(\tau)}{\tau - t} \mathrm{d}\tau \tag{1}$$

$$x(t) = H^{-1}[\bar{x}(t)] = \frac{1}{\pi} P \int_{-\infty}^{\infty} \frac{\bar{x}(\tau)}{\tau - t} \mathrm{d}\tau \tag{2}$$

These integrals are improper integrals in the sense of the Cauchy principal value denoted by P. Equation (2) yields

$$x(t) = \lim_{\varepsilon \to 0; A \to \infty} \frac{1}{\pi} \left\{ \int_{-A}^{t-\varepsilon} (\cdot) \mathrm{d}\tau + \int_{t+\varepsilon}^{A} (\cdot) \mathrm{d}\tau \right\} \tag{3}$$

The Hilbert transform described by Eqs. (1) and (2) are frequently written in terms of convolution notation:

$$\bar{x}(t) = \frac{1}{\pi t} * x(t) \tag{4}$$

$$x(t) = -\frac{1}{\pi t} * \bar{x}(t) \tag{5}$$

The functions $x(t)$ and $\bar{x}(t)$ are called a pair of Hilbert transforms and are denoted by

$$x(t) \Leftrightarrow^{H} \bar{x}(t) \tag{6}$$

The complex signal for which the imaginary part is the Hilbert transform of the real part is called the analytic signal; that is, an analytic signal $X(t)$ is formulated as

$$X(t) = x(t) + j \cdot \bar{x}(t) = A(t) e^{j\theta} \tag{7}$$

where

$$\begin{cases} A(t) = \sqrt{x^2(t) + \bar{x}^2(t)} \\ \theta(t) = tg^{-1}\left(\frac{\bar{x}(t)}{x(t)}\right) \end{cases} \tag{8}$$

The instantaneous frequency of the signal is defined as

$$\omega(t) = 2\pi f(t) = \frac{\mathrm{d}\theta(t)}{\mathrm{d}t} \tag{9}$$

or

$$\omega(t) = \frac{\mathrm{d}}{\mathrm{d}t}\left(tg^{-1}\frac{\bar{x}(t)}{x(t)}\right) = \frac{x(t)\dot{\bar{x}}(t) - \dot{x}(t)\bar{x}(t)}{x^2(t) + \bar{x}^2(t)} = \frac{x(t)\dot{\bar{x}}(t) - \dot{x}(t)\bar{x}(t)}{A^2(t)} \tag{10}$$

B. Nonlinear Parameter Identification from Dynamic System Free Response

By using the Hilbert transform, we can identify the linear damping parameter from an impulse response function. It has been demonstrated that this technique possesses some advantages, especially when the frequency-domain resolution is limited [2].

Here, considering a more general single-degree-of-freedom (SDOF) system, its free-vibration response with viscous damping is governed by

$$m(t)\ddot{x}(t) + c(t)\dot{x}(t) + k(t)x(t) = 0 \tag{11}$$

On the condition that m is time-invariant, Eq. (11) can be written as

$$\ddot{x}(t) + 2h_0(t)\dot{x}(t) + \omega_0^2(t)x(t) = 0 \tag{12}$$

where $h_0(t) = c(t)/2m$ is the viscous damping coefficient, and $\omega_0(t) = \sqrt{k(t)/m}$ is the undamped natural frequency. In [7], a general approach of nonlinear transient-vibration analysis using Hilbert transform for the system described by Eq. (12) was developed. In what follows, we briefly outline the key results provided by Feldman [7] that are relevant to the present study.

Based on the Bedrosian [15] theorem, when two functions [say, $x(t)$ and $h_0(t)$] are signals with nonoverlapping spectra and the spectrum of the $h_0(t)$ is lower than that of $x(t)$, then we have

$$H[h_0(t)x(t)] = h_0(t)H[x(t)]$$

We then perform Hilbert transform for Eq. (12). In virtue of Eq. (7), we can obtain

$$\ddot{X}(t) + 2h_0(A)\dot{X}(t) + \omega_0^2(A)X(t) = 0 \tag{13}$$

by substituting the expressions of $X(t)$ and its derivatives $\dot{X}(t)$ and $\ddot{X}(t)$ into Eq. (13) and then separating the real and imaginary parts of Eq. (13), we can obtain the expressions for the instantaneous undamped natural frequency and the instantaneous damping characteristic:

$$\begin{cases} \omega_0^2 = \omega^2 - \frac{\ddot{A}}{A} + \frac{2\dot{A}^2}{A^2} + \frac{\dot{A}\dot{\omega}}{A\omega} \\ h_0 = -\frac{\dot{A}}{A} - \frac{\dot{\omega}}{2\omega} \end{cases} \tag{14}$$

For a system with structural damping, as pointed out in [7], the Hilbert transform of the free-vibration equation is

$$\ddot{X}(t) + \omega_0^2(A)\left[1 + j\frac{\delta(A)}{\pi}\right] = 0 \tag{15}$$

where δ is the logarithmic decrement. The corresponding system parameters are

$$\begin{cases} \omega_0^2 = \omega^2 - \frac{\ddot{A}}{A} \\ \delta = -\frac{2\pi\dot{A}\omega}{A\omega_0^2} - \frac{\pi\dot{\omega}}{\omega_0^2} \end{cases} \tag{16}$$

III. Practical Issues and Solutions of the Discrete Hilbert Transform in Engineering Applications

When performing a Hilbert transform to a perfect signal, high-fidelity results are readily generated. However, when dealing with experimentally obtained data, because they are usually polluted by noise, it is not guaranteed to get results as expected. Thus, additional signal preprocessing is usually needed to get desirable results from noisy engineering data.

A. Noise Rejection

With a pure analytical signal [for example, a sine wave $x(t)$, as shown in Fig. 1a], its Hilbert transform $\bar{x}(t)$ can be found analytically. From the analytic function $X(t) = x(t) + j\bar{x}(t)$, we can find the phase, as seen in Fig. 1b. By definition, numerical derivation of the phase with respect to time is the instantaneous frequency. This process of finding the instantaneous frequency is sufficient for a signal without noise. In many engineering applications, the signal is obtained experimentally, and thus the signal usually contains noise. With even minor noise present in a signal, operations such as numerical differentials may result in an erroneous conclusion.

For example, as shown in Fig. 2a, a pure sine signal is added with 1% uniform random noise. With such a minor level of noise pollution, it is barely visible from the signal itself and from the corresponding Hilbert transform. Similarly, the noise level in the phase is also small in relative amplitude. However, by applying the first-order time derivative to the phase to get the frequency, the noise has been significantly amplified, as seen in Fig. 2b. In fact, the noise becomes the dominant signal.

To extract meaningful information, denoising techniques are usually required in such engineering applications. For this particular example, because we know the noise and signal properties in advance, a curve fitting to the phase information can achieve a good result (Fig. 3a). In cases with an unknown signal property, different denoise techniques can be applied, such as wavelet transform denoising (Fig. 3b) or filtering (Fig. 3c), in which the noise has been significantly suppressed.

B. Errors in the DHT-Based Envelope Detection

When applying the DHT in system parameter identifications, it usually requires the envelope and the corresponding time derivatives [7,9]. For a discrete-time signal, its Hilbert transform is usually calculated by applying the FFT and the inverse FFT (IFFT) to the signal and extracting the analytic function directly [13].

According to [13], the discrete analytic signal for a sequence $x(n)$ can be calculated with the following steps:

1) Compute the N-point DTFT $X(n)$ using FFT of the N real-valued data sample $x(n)$.

2) Form the N-point one-sided data series from $X(n)$:

$$Z(n) = \begin{cases} X(1), & \text{for } n = 1 \\ 2X(n), & \text{for } 2 \le n \le \frac{N}{2} \\ X\left(\frac{N}{2}+1\right), & \text{for } n = \frac{N}{2}+1 \\ 0, & \text{for } \frac{N}{2}+2 \le n \le N \end{cases}, \quad \text{for even } N \text{ case}$$

or

$$Z(n) = \begin{cases} X(1), & \text{for } n = 1 \\ 2X(n), & \text{for } 2 \le n \le \frac{N+1}{2} \\ 0, & \text{for } \frac{N+1}{2}+1 \le n \le N \end{cases}, \quad \text{for odd } N \text{ case}$$

3) Compute the inverse DTFT of the N-point series $Z(n)$ to get the complex discrete-time analytic signal $z(n)$ of the same sample rate as the original signal $x(n)$.

Because the discrete Fourier transform assumes the repetition of the signal infinitely in the time domain, significant inaccuracy can occur, especially at both edges of the signal. This kind of inaccuracy can be further amplified after derivatives.

For the simplicity of explanation, let us take an simple example of

$$x(t) = e^{-\sigma t}\cos\omega t \tag{17}$$

where $\sigma = \xi\omega$. To further simplify the statement, we assume that the signal is a response from a time-invariant system; thus, both ξ and ω are constant. For such a case, we know the exact Hilbert transform as

$$\bar{x}(t) = e^{-\sigma t}\sin\omega t \tag{18}$$

and the envelope

$$A(t) = e^{-\sigma t} \tag{19}$$

To have a numerical example, we assign $\omega = 10\pi$ and $\sigma = 0.5\pi$ for the purpose of illustration. When the signal is digitized with a sampling rate of 1000 Hz, the digitized signal is as shown in Fig. 4. Its corresponding discrete Hilbert transform can be readily calculated by an FFT- and IFFT-based algorithm, such as the algorithm provided by MATLAB. The envelope, the instantaneous phase, and the instantaneous frequency of the digitized signal are calculated and plotted in Fig. 5. The exact solution is also plotted in the figure for comparison. In the figure, the solid lines are the HDT solutions and the dashed lines are the exact solutions. As seen in the figure, the error induced by the DHT method is significant, especially at the edges. The error is even more significant in the instantaneous frequency, due to the amplification factor introduced by the numerical derivation.

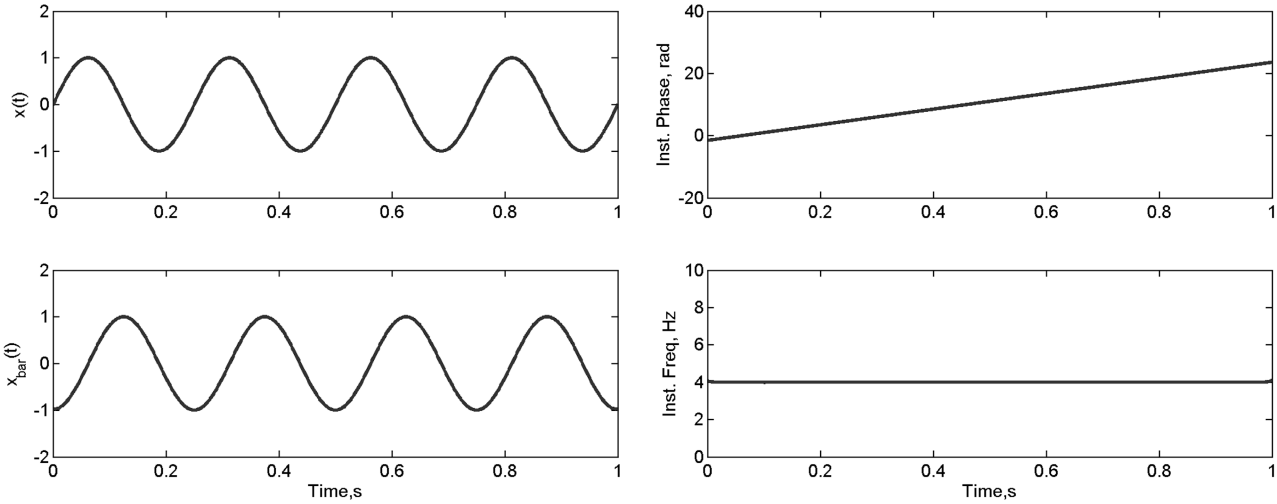

a) Signal and its Hilbert transform

b) Instantaneous phase and frequency

Fig. 1 Hilbert transform of a pure sine signal.

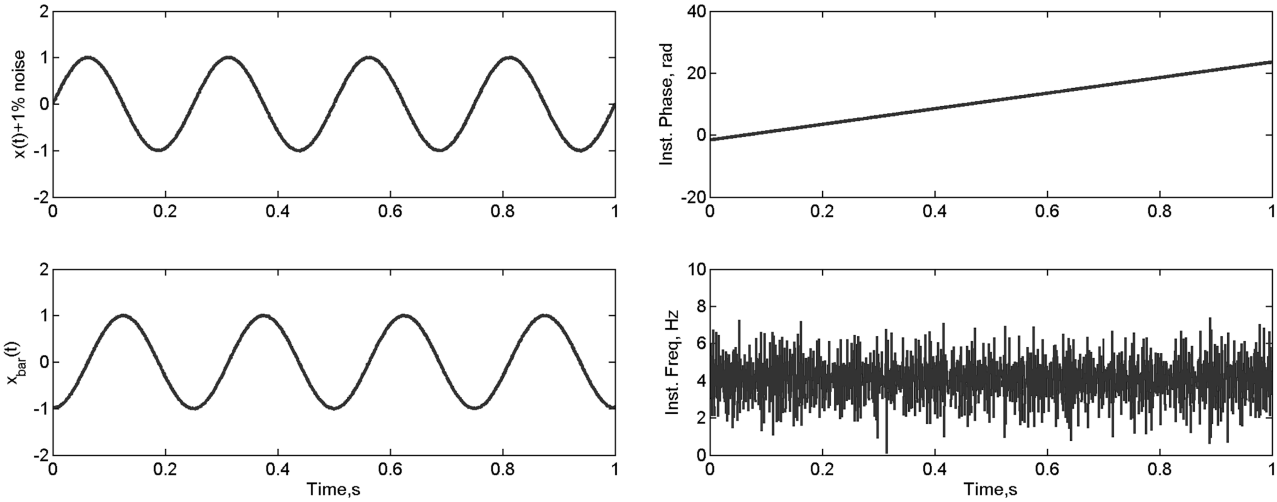

a) Signal with 1% noise and its Hilbert transform **b) Instantaneous phase and frequency**

Fig. 2 Hilbert transform of a pure sine signal with noise.

C. Local-Maxima-Interpolation Method

To reduce the errors in the FFT- and IFFT-based discrete Hilbert transform, we developed an algorithm for envelope detection based on the LMI. The basic procedures of the LMI include two major steps:

1) For a given signal, the local maxima are detected first, as shown in Fig. 6.

2) The local maxima are spline fit to approximate the envelope, as shown in Fig. 7.

Generally, this approach is an approximation. It is exact only in special cases, such as in the zero-damping case. For a simple case, as shown in Eq. (17), the signal value $x(t)$ takes the exact envelope values $A(t)$ at locations when

$$\cos \omega t = 1 \tag{20}$$

or

$$\omega(t_n)t_n = 2n\pi, \qquad n = 0, 1, \ldots \tag{21}$$

Whereas in the local-maxima-approximation approach, those locations were determined by solving

$$\frac{\mathrm{d}[x(t)]}{\mathrm{d}t} = 0 \tag{22}$$

or

$$\dot{A} \cos \omega t - A(\omega + \dot{\omega}t) \sin \omega t = 0 \tag{23}$$

or

$$\sin(\omega t - \phi) = 0 \tag{24}$$

where

$$\phi = tg^{-1}\left(\frac{\dot{A}}{A(\omega + \dot{\omega}t)}\right) \tag{25}$$

The local maxima lie at

$$\omega(t_{na})t_{na} - \phi(t_{na}) = 2n\pi, \qquad n = 0, 1, \ldots \tag{26}$$

Apparently, the approximate solution t_{na} obtained from Eq. (26) is generally different from the exact solution t_n obtained from Eq. (21). The approximation $t_{na} \approx t_n$ is valid only when $[\dot{A} \ll A(\omega + \dot{\omega}t)]|_{t=t_n}$. The approximation solution becomes an exact solution only when $\dot{A} = 0$ (i.e., in a situation of a constant envelope).

In a case of Eq. (17) with constant parameters σ and ω, we have

$$\dot{A} = -\sigma A \quad \text{and} \quad \dot{\omega} = 0 \tag{27}$$

Thus, by substituting Eq. (27) into Eq. (28), we have

$$\phi = tg^{-1}\left(\frac{-\sigma}{\omega}\right) = tg^{-1}(-\xi) = -tg^{-1}(\xi) \tag{28}$$

Substituting Eq. (28) into Eq. (26), we get

$$\omega t_{na} = 2n\pi - tg^{-1}(\xi), \qquad n = 0, 1, \ldots \tag{29}$$

or

$$t_{na} = \frac{2n\pi}{\omega} - \frac{tg^{-1}(\xi)}{\omega} = t_n - \frac{tg^{-1}(\xi)}{\omega}, \qquad n = 0, 1, \ldots \tag{30}$$

Equation (30) indicates that the approximation method is lagging behind the exact solution when the damping is small and positive. On the other hand, if the damping is small but negative, the approximation solution is leading ahead of the exact solution. For a case of Eq. (17) with constant parameters, this conclusion can be easily seen in Fig. 8a for a small positive-damping ratio and in Fig. 8b for a small negative damping. In both figures, the solid lines are the signals, the dashed lines are the true envelopes, the dashed-dotted lines are the LMI envelopes, the circles are the local maxima, and the squares are the true-envelope solutions.

In either the positive- or negative-damping case, the LMI method gives an underestimation of the envelope. Nevertheless, the LMI method has greatly improved the envelope detection compared with the results by the DHT based on the FFT and IFFT techniques. In Fig. 9, we have shown the relative errors between the true envelope and the envelope detected by the LMI method and by the FFT- and IFFT-based method. In the figure, the circles are the relative error from the DHT, and the dashed line is the relative error from the LMI approach. In the figure, the relative error is defined as

$$\text{error}\,(t) = \frac{\text{estimated envelope}\,(t) - \text{true envelope}\,(t)}{\max\ (\text{true envelope})} \times 100\% \tag{31}$$

From Fig. 9, it is seen that with the FFT- and IFFT-based DHT, the errors are large at the edges. For this particular case, the error at the beginning reaches to 60%, whereas the error at the end is over 100%. Whereas by using the LMI method, the edge error is reduced down to less than 0.4%. The LMI method also reduces the fictitious oscillation in the middle of the time domain (Fig. 10). These kinds of erroneous oscillations are especially susceptible to noise in time derivatives.

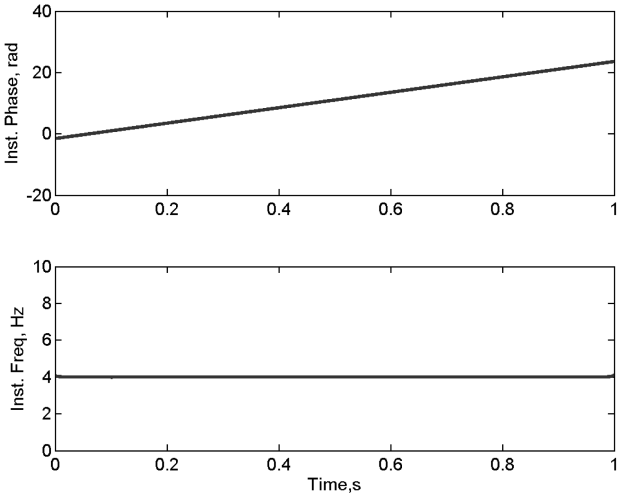

a) Curve-fitting denoising

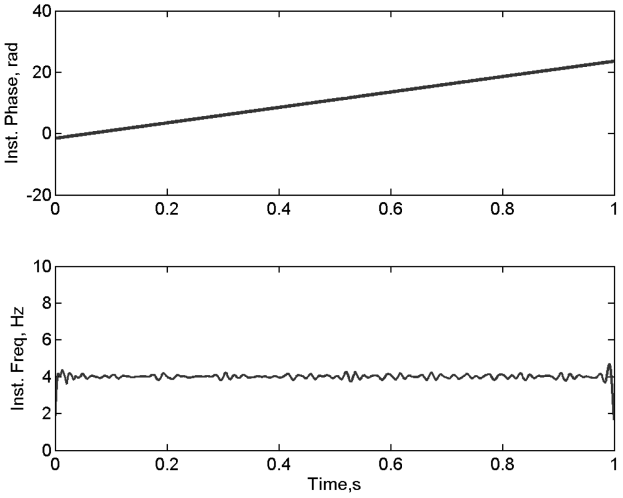

b) Wavelet-transform-based denoising

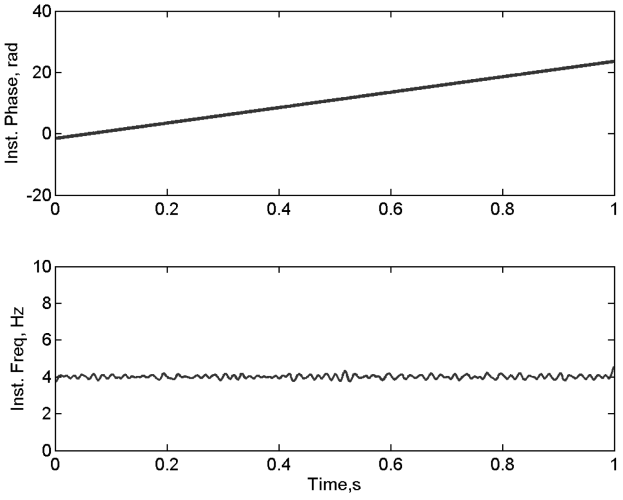

c) Low-pass filtering

Fig. 3 Denoising techniques.

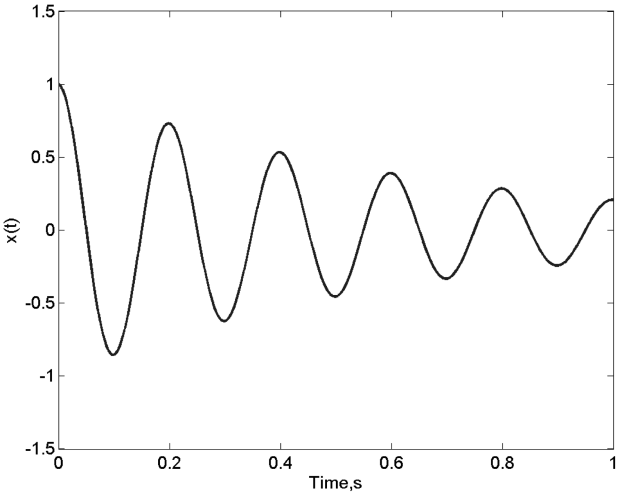

Fig. 4 Signal $x(t) = e^{-0.5\pi t} \cos 10\pi t$.

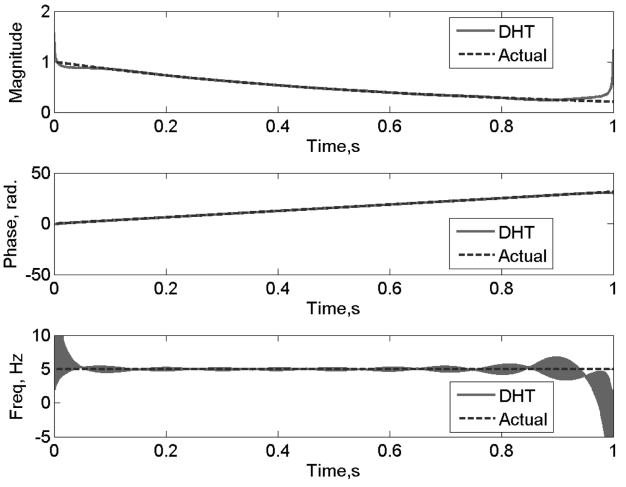

Fig. 5 Analytic function amplitude, phase, and corresponding frequency of the DHT and exact solution (actual).

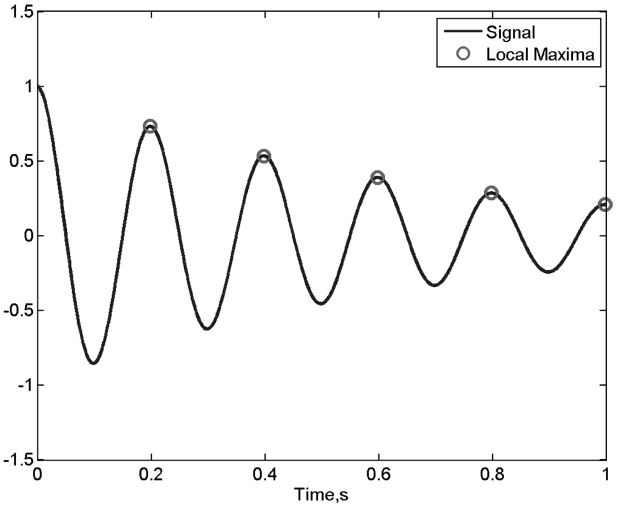

Fig. 6 Local-maxima detection.

To further examine the advantages of the LMI method, the simulations to Eq. (17) are extended to a larger damping range of from −10 to 10%. In Fig. 11, the largest error is plotted against the damping ratio. For each damping value, the largest error is defined as the largest deviation of the detected envelope from the true-envelope values within the simulation time interval. In the figure, the circles are the error from the FFT- and IFFT-based approach, and the dots are the error from the LMI method. As clearly seen from the figure, the LMI method has significantly improved the envelope detection for all damping ratios. Compared with the 145% error with the conventional DHT, the largest error from the LMI method reduces to

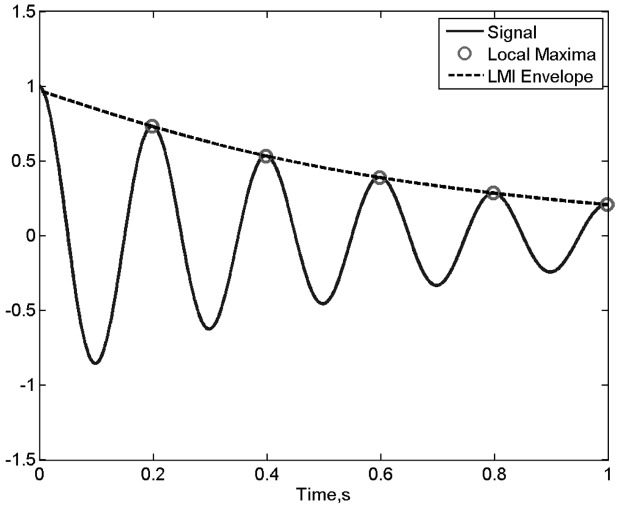

Fig. 7 Envelope detection.

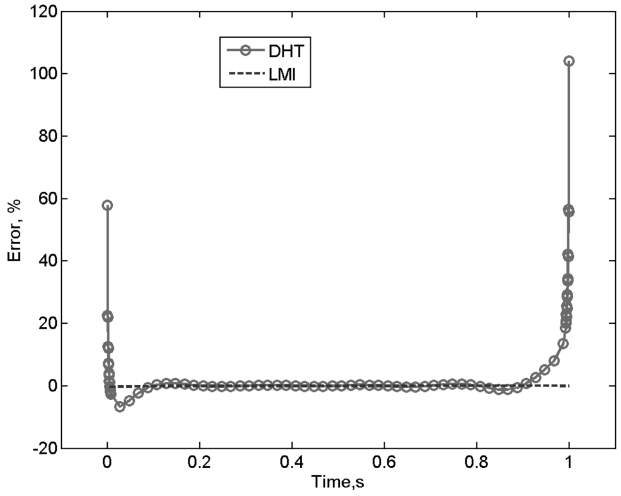

Fig. 9 Relative errors.

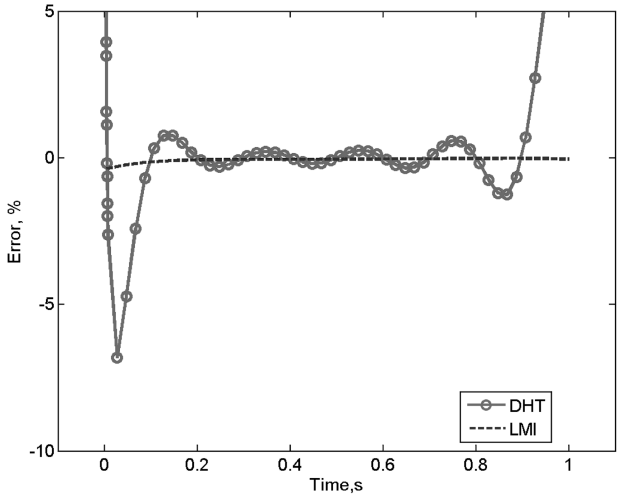

Fig. 10 Relative errors, zoomed view.

less than 3%. At zero damping (i.e., the signal is a pure sinusoid), both methods reach zero error, as expected from Eq. (25) and the consequent explanations after that.

IV. Industrial Application

In modern industrial designs, nonlinear behaviors of dynamic system response have been taken into consideration. For example, nonlinear friction has been used to enhance engine blade damping, and wire-mesh-bearing dampers have been designed for improving rotor dynamics stability. Nonlinear system characterization for industrial systems becomes a very active and challenging topic. In this application, we choose two examples for demonstrating the effectiveness of the proposed LMI methods under both low-damping and high-damping scenarios. The first example is a baseline blade without additional friction damping treatment, which has very small damping. The second example is a recently developed wire-mesh damper, which is a nonlinear dynamic system and possesses high equivalent damping.

A. Low-Damping Blade

In this case, the damping mechanism is mainly due to blade material damping; thus, the damping value is very small. However, due to the fact that the blade is clamp-mounted, friction may occur at the blade root, and the boundary condition may slightly change under large vibration levels. Therefore, weak nonlinearity still exists in frequency and damping.

The blade was first excited at one of its resonance by a noncontact shaker, and then the excitation was cut off by shutting down the power supply to the shaker. The free response of the blade was picked

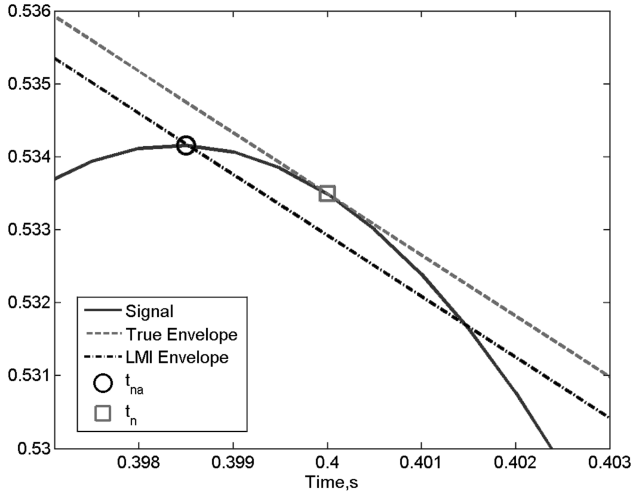

a) Positive damping

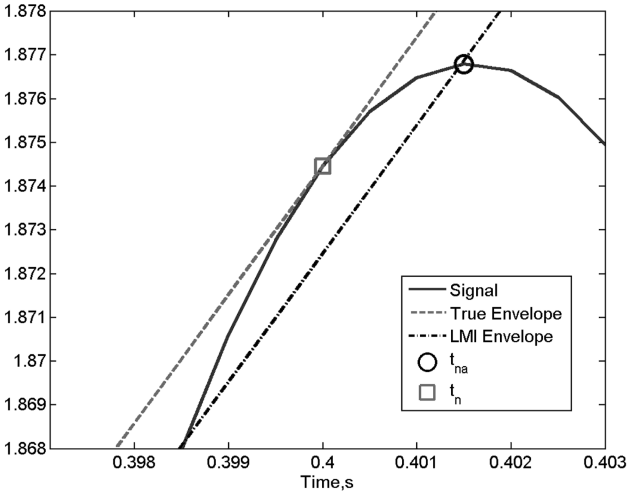

b) Negative damping

Fig. 8 Error source of the envelope detected by the local-maxima method.

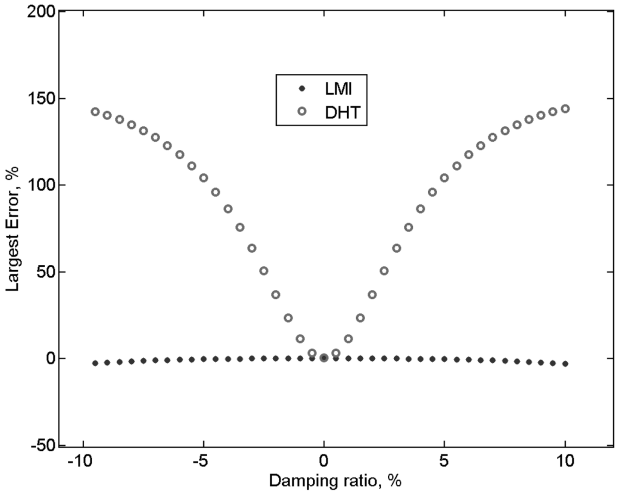

Fig. 11 Envelope error vs damping ratio.

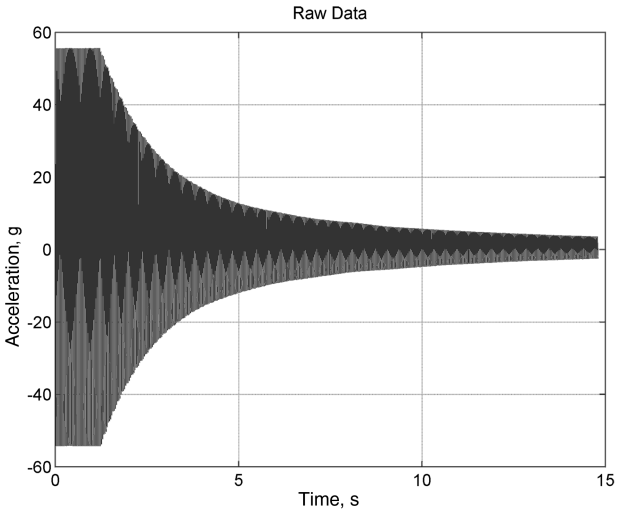

Fig. 12 Blade free response.

up by an accelerometer, as shown in Fig. 12. The data were then used for system identification, described in Sec. II with the LMI envelope detection. In the data processing, the forced-response portion of the data was cut off. Modal responses other than the mode of interest were also removed using the empirical modal decomposition method [4].

The identified frequency and equivalent damping as functions of time are shown in Fig. 13. The top portion of the figure is the identified frequency, and the bottom portion is the equivalent damping ratio. It is seen from the figure that the identified frequency increases slightly with time, whereas the identified damping ratio is very small and decreases with time. When those parameters are plotted as functions of vibration amplitude, as seen in Fig. 14, it is clearly indicated that the system behaves as a system with a stiffness-softening spring, and the identified damping is small but increases with vibration amplitude.

To assess the identification quality, we reconstruct the time history based on the identified parameters, frequency and damping ratio as

$$x_{\text{reconstruction}}(t) = \text{Re}[x_{\text{denoised}}(t) + jx_{\text{Hibert transform}}(t)] = \text{Re}[A(t)e^{j\theta(t)}] \tag{32}$$

Then the reconstructed time history is compared with the denoised response data according to the following measure:

$$\text{error} = \frac{\Delta x^T \Delta x}{(x^T_{\text{reconstructed}} x_{\text{denoised}})^{\frac{1}{2}} (x^T_{\text{denoised}} x_{\text{denoised}})^{\frac{1}{2}}} \times 100\% \tag{33}$$

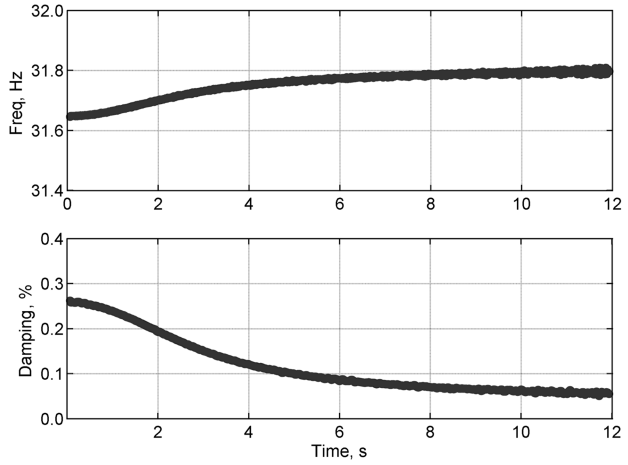

Fig. 13 Identified blade frequency and damping as functions of time.

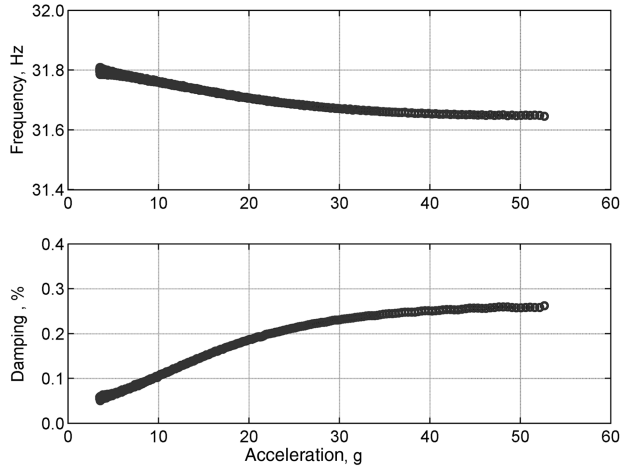

Fig. 14 Identified blade frequency and damping as functions of vibration amplitude.

where Δx is the difference between the denoised time history and the reconstructed time history:

$$\Delta x(t) = x_{\text{reconstructed}}(t) - x_{\text{denoised}}(t)$$

By using this error definition, we can easily build a model from the identified parameters and achieve relative errors below 0.1% for this case. Figure 15 shows comparisons between the reconstructed data and the denoised free response. The zoomed version comparisons of the first 0.2 s data are shown in Fig. 16, which also indicates very good agreement.

B. Wire-Mesh Damper

Wire-mesh dampers are potentially a good replacement for squeeze-film dampers as bearing-support dampers. Wire-mesh dampers have shown amplitude-dependent nonlinear dynamic characteristics. Previous studies have used the frequency-domain-based method to successfully characterize a wire-mesh damper [16]. However, those methods typically require tedious tests to scan in the frequency range of interest while carefully controlling test parameters such as vibration amplitude and excitation frequency. The DHT-based method for identifying nonlinear stiffness and damping parameters for wire-mesh dampers has been used in the past.

With the DHT-based method, the dynamic characteristics of wire-mesh dampers are determined through its impulse response. As shown in Fig. 17, the impulse was generated through an instrumented

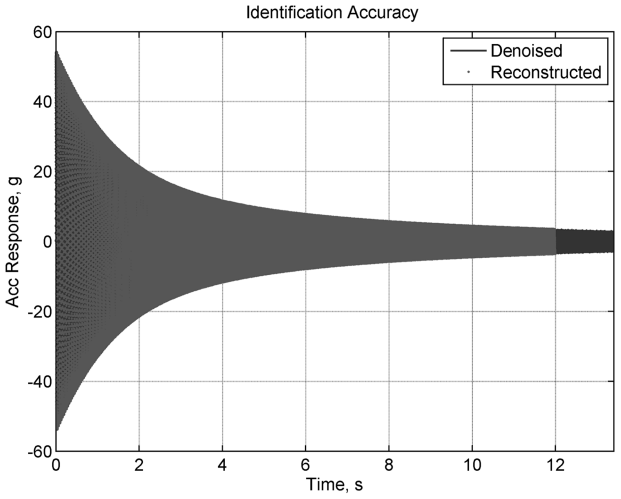

Fig. 15 Comparisons between reconstruction and denoised responses.

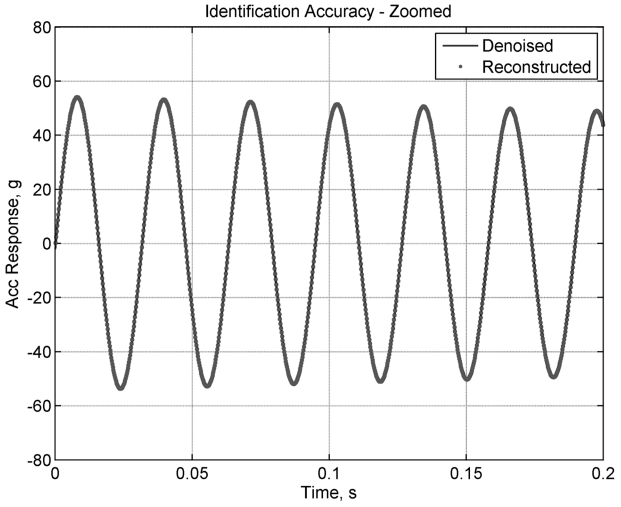

Fig. 16 Comparisons between reconstruction and denoised responses, zoomed.

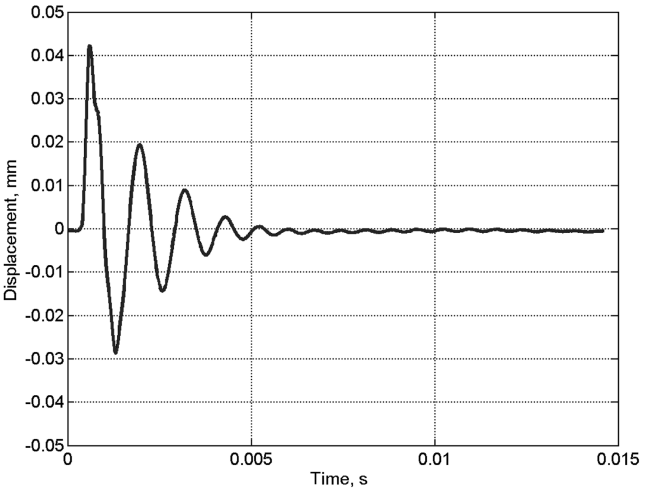

Fig. 18 Sensor response.

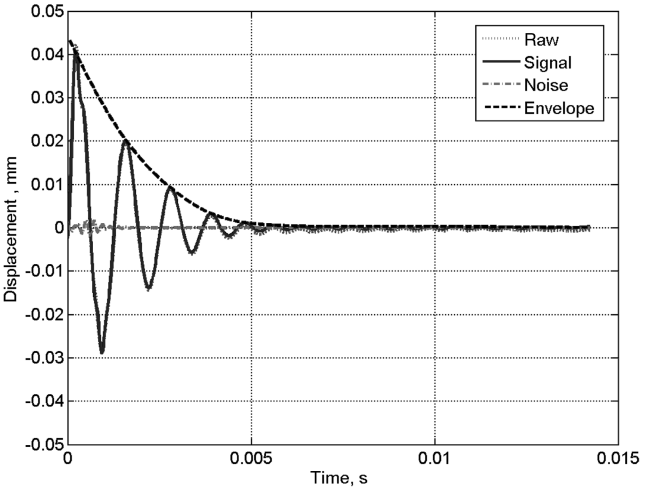

Fig. 19 Envelope detection.

hammer, and the impulse response was measured by a vibration sensor (a proximity probe in this case).

A typical response is shown in Fig. 18. The response is dominated by the fundamental mode response; nevertheless, because the response is excited by an impulse hammer, minor higher-order modal responses may have also been excited. Thus, a denoising technique was applied to the response data before the envelope detection.

In this investigation, a wavelet-transformation-based denoising technique was used. In Fig. 19, the dashed-dotted line is the isolated high-frequency noise. Because the noise is mainly in the higher-frequency range, the noise is concentrated at the beginning of the response, as expected. The LMI method is then applied to the denoised response to obtain the envelope, which is plotted as the dashed line in the figure.

With the procedures described in Sec. II, we can derive the system frequency and equivalent damping ratio, as shown in Figs. 20 and 21, respectively. Both frequency and damping ratio show vibration-amplitude dependency.

By using the same error definition in Eq. (33), the fitting error for this case reaches below 3%. The comparison between the reconstructed data and the denoised response is illustrated in Fig. 22, which shows a very good agreement as well.

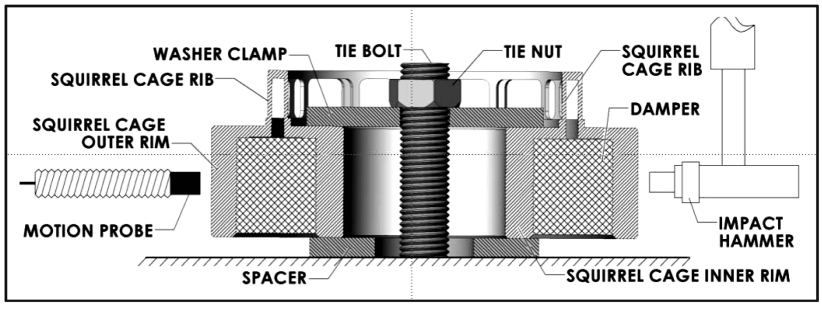

Fig. 17 Wire-mesh damper and the test setup.

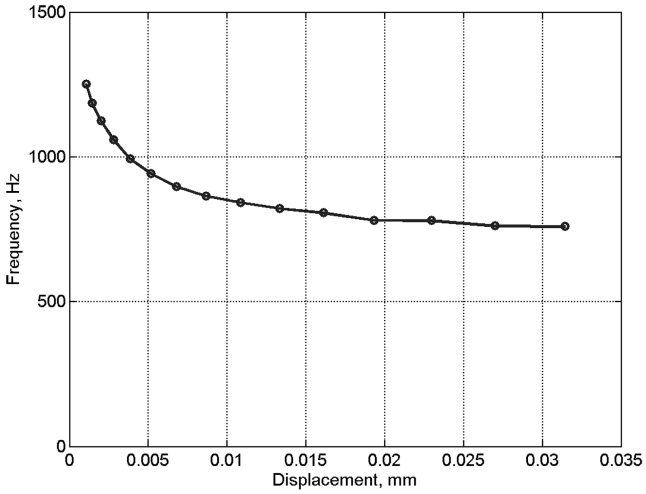

Fig. 20 Identified frequency.

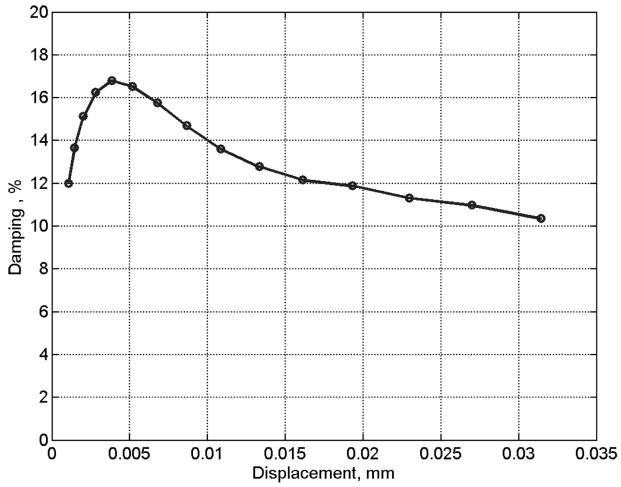

Fig. 21 Identified damping ratio.

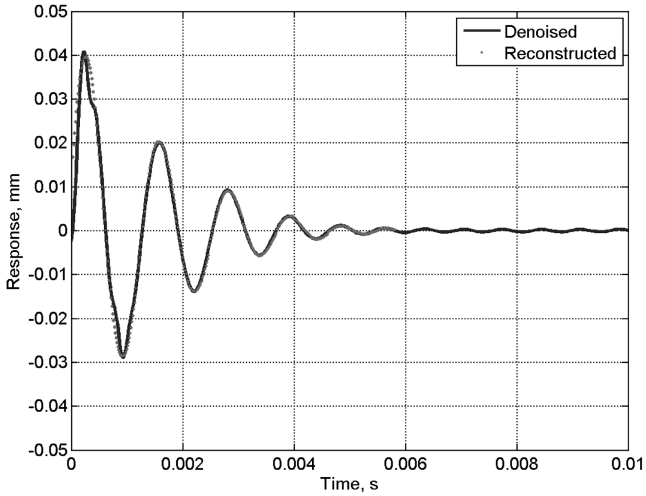

Fig. 22 Reconstruction.

V. Conclusions

The Hilbert transform can be a useful tool for dynamic system identification and characterizations, especially when considering nonlinear systems. Because the identification procedure involves derivatives of the Hilbert transform, it requires high accuracy in the DHT. There are two major noise sources when applying the DHT-based analysis to solve an engineering problem. The first one is the noise introduced during the data acquisition. This can be the digitization noise, data-reduction noise, and modeling noise. The second source is from the DHT algorithms. Because of limitations inherent to the discrete Fourier transform, the conventional DHT obtained by FFT and IFFT algorithms usually contains inaccuracies. The noise may be minor in regular analyses, but in nonlinear parameter identifications, it can be overwhelming after numerical derivations. This noise effect is especially severe at both ends of the time history, even in numerically simulated time histories. As a result, the conventional Hilbert transform is not reliable at both ends. It could hinder the application of the Hilbert transform in many engineering applications, especially to systems with large damping.

The LMI-based Hilbert enveloping-detection algorithm proposed in this paper is an alternative method for the FFT- and IFFT-based DHT analysis. Although the LMI-based algorithm is simple and easy to implement, it greatly suppresses the envelope-detection error induced by FFT and IFFT in the conventional Hilbert transform. Analyses indicate that the LMI-based method slightly underestimates the true Hilbert envelope. Numerical simulations indicate that the LMI-based method is much more accurate than the FFT- and IFFT-based approach. Applications of the LMI approach to the practical examples demonstrated that the method could successfully identify small and large damping in linear/nonlinear systems.

References

[1] Simon, M., and Tomlinson, G. R., "Use of the Hilbert Transform in Modal Analysis of Linear and Nonlinear Structures," *Journal of Sound and Vibration*, Vol. 96, No. 4, 1984, pp. 421–436. doi:10.1016/0022-460X(84)90630-8

[2] Thrane, N., Wismer, J., Konstantin-Hansen, H., and Gade, S., "Practical Use of the 'Hilbert Transform,'" Brüel & Kjaer, Application Note BO0437-11, Denmark, 1997 http://www.bksv.com/doc/bo0437.pdf [retrieved Jan. 2009].

[3] Huang, N. E., Zheng, S., Long, S. R., Wu, M. C., Shih, H. H., Zheng, Q., Yen, N.-C., Tung, C. C., and Liu, H. H., "The Empirical Mode Decomposition and the Hilbert Spectrum for Nonlinear and Nonstationary Time Series Analysis," *Proceedings of the Royal Society of London, Series A: Mathematical and Physical Sciences*, Vol. 454, No. 1971, 1998, pp. 903–995. doi:10.1098/rspa.1998.0193

[4] Huang, N. E., and Shen, S. S. P., *Hilbert-Huang Transform and Its Applications*, World Scientific, Singapore, 2005.

[5] Feldman, M., "Time-Varying Vibration Decomposition and Analysis Based on the Hilbert Transform," *Journal of Sound and Vibration*, Vol. 295, Nos. 3–5, 2006, pp. 518–530. doi:10.1016/j.jsv.2005.12.058

[6] Feldman, M., "Theoretical Analysis and Comparison of the Hilbert Transform Decomposition Methods," *Mechanical Systems and Signal Processing*, Vol. 22, No. 3, 2008, pp. 509–519. doi:10.1016/j.ymssp.2007.09.013

[7] Feldman, M., "Nonlinear System Vibration Analysis Using Hilbert Transform, 1: Free Vibration Analysis Method 'FREEVIB,'" *Mechanical Systems and Signal Processing*, Vol. 8, No. 2, 1994, pp. 119–127. doi:10.1006/mssp.1994.1011

[8] Feldman, M., "Nonlinear System Vibration Analysis Using Hilbert Transform 2: Forced Vibration Analysis Method 'FORCEVIB,'" *Mechanical Systems and Signal Processing*, Vol. 8, No. 3, 1994, pp. 309–318. doi:10.1006/mssp.1994.1023

[9] Allara, M., Filippi, S., and Gola, M., "An Experimental Method for the Measurement of Blade root Damping," ASME Turbo Expo 2006, American Society of Mechanical Engineers, Paper GT-2006-90774, 2006.

[10] Luo, H., Fang, X., Hallman, D., and Tang, J., "Characterization of Particle Damper Using Hilbert Transform and Free Vibration Response," 48th AIAA/ASME/ASCE/AHS/ASC Structures, Structural Dynamics, and Materials Conference, Honolulu, HI, AIAA Paper 2007-2048, Apr. 2007.

[11] Fang, X., Luo, H., and Tang, J., "Investigation of Granular Damping in Transient Vibrations Using Hilbert-Transform-Based Technique," *Transactions of the ASME; Journal of Vibration and Acoustics*, Vol. 130, No. 3, 2008, Paper 031006. doi:10.1115/1.2827454

[12] Pai, P. F., and Palazotto, A. N., "Detection and Identification of Nonlinearities by Amplitude and Frequency Modulation Analysis," *Mechanical Systems and Signal Processing*, Vol. 22, No. 5, 2008, pp. 1107–1132. doi:10.1016/j.ymssp.2007.11.006

[13] Marple, S. L., Jr., "Computing the Discrete-Time Analytic Signal via FFT," *IEEE Transactions on Signal Processing*, Vol. 47, No. 9, 1999, pp. 2600–2603. doi:10.1109/78.782222

[14] Hahn, S. L., *Hilbert Transforms in Signal Processing*, Artech House, Boston, 1996.

[15] Bedrosian, E., "A Product Theorem for Hilbert Transforms," *Proceedings of the IEEE*, Vol. 51, No. 5, May 1963, pp. 868–869. doi:10.1109/PROC.1963.2308

[16] Ertas, B., and Luo, H., "Nonlinear Dynamic Characterization of Oil Free Wire Mesh dampers," *Journal of Engineering for Gas Turbines and Power*, Vol. 130, No. 3, May 2008, Paper 032503. doi:10.1115/1.2836744

J. Cooper
Associate Editor